PRELIMINARY NOAA-15 HIRS/3 RADIANCE VALIDATION FROM HIGH SPECTRAL RESOLUTION AIRCRAFT OBSERVATIONS.

Paul van Delst
Cooperative Institute of Meteorological Satellite Studies
University of Wisconsin-Madison
Madison WI, USA

1. INTRODUCTION

Typically once meteorological spacecraft are launched there are no means to validate the calibration of the on-board sensors in an absolute manner. With the advent of well calibrated, high spectral resolution aircraft instruments that are deployed regularly, the opportunity to use these aircraft instruments to vicariously calibrate infrared (IR) and microwave (MW) satellite sensors, such as those on NOAA-15, presents itself. This paper details results from data gathered at the Wallops98 field experiment where the NASA ER-2, carrying a high-resolution IR spectrometer, flew over the ocean off the East coast of the United States in clear sky conditions timed to coincide with the overpass of the NOAA-15 polar orbiting satellite.

2. VALIDATION METHODOLOGY

Comparison of collocated HIRS/3 and high spectral resolution aircraft measurements requires the high resolution data to be spectrally averaged over the HIRS/3 channel response,

$$\overline{R}_{HiRes} = \frac{\int_{\nu_1}^{\nu_2} R_{HiRes}(\nu) SRF_{HIRS}(\nu) d\nu}{\int_{\nu_1}^{\nu_2} SRF_{HIRS}(\nu) d\nu} \tag{1}$$

where $R_{HiRes}(\nu)$ is the high resolution aircraft radiance measurement and $SRF(\nu)$ is the HIRS/3 spectral response function.

A correction needs to be applied to both the HIRS/3 and high resolution data to account for the differences in viewing height and angle between the two instruments. To do this, each instrument's measurement is simulated from a calculated high resolution radiance spectrum. The calculated radiances are then differenced and this difference is used as a correction to the observed radiances,

$$\Delta R = \left(\overline{R}_{HiRes} - R_{HIRS}\right)_{OBS} - \left(\overline{R}_{HiRes} - R_{HIRS}\right)_{CALC} \tag{2}$$

This avoids modifying the measurements directly to get one instrument's observation to approximate that of the other. The disadvantage of this method is that it relies on the ability to simulate instruments with good accuracy. This can be problematic if the in situ data, e.g. sonde profiles, used in the forward calculation has itself not been validated or if there is poor collocation of the in situ, satellite and aircraft measurements.

3. FIELD EXPERIMENTS DATASET

3.1 Satellite and aircraft data

During the Wallops98 field experiment (June 24 – July 15, 1998) based at the NASA Wallops Flight Facility, the ER-2 instrument complement of interest to NOAA-15 sensor validation activities consisted of the High-resolution Interferometer Sounder (HIS) (*Revercomb et al*, 1988) and the NPOESS Aircraft Sounder Testbed Interferometer (NAST-I) (*Cousins and Smith*, 1997. Also, *Revercomb et al*, 1998). The nadir viewing HIS and the cross-track scanning NAST-I measure upwelling infrared (IR) radiation from 3-8-16μm and 3.3-16.7μm at spectral resolutions of 0.5-1.0cm^{-1} and 0.25cm^{-1} respectively. There were no microwave instruments on board the ER-2 during Wallops98 so the validation opportunity exists for the HIRS/3 instrument only.

Two missions were flown with the ER-2 underflying the NOAA-15 spacecraft in clear sky conditions – on July 11 and 14, 1998. HIS calibrated radiances are available only for the July 11 mission (the instrument failed during the July 14 flight) and NAST-I calibrated radiances are not yet available for analysis. Only HIS Band I (600-1100cm^{-1}) radiances will be examined here as comparisons between the HIS and initially processed NAST-I data show a bias in the HIS mid- and shortwave bands (1100-2700cm^{-1}) thought to be due to scattering off the HIS scene mirror. The MODIS Airborne Simulator (MAS) was also aboard the ER-2 to provide a qualitative assessment of the cloudiness of the scenes of interest. The coincidence of the NOAA-15 nadir track and the ER-2 flight track for the July 11 mission is shown in figure 1. The data times of interest are 12:29-12:47UTC (NE heading leg) and 12:51-13:09UTC (SW heading leg). The ER-2 and NOAA-15 were temporally collocated halfway through the NE leg at approximately 12:37UTC. Sondes were released from the Wallops Flight Facility at 14:52 and 15:54UTC.

To validate the HIRS/3 channels with the aircraft radiances, cloud free conditions are a necessary requirement. The GOES-8 Imager 4km visible image for 12:45UTC on July 11 showed clear skies over the region of interest with bands of stratus to the south and far north of the NE/SW flight legs. The 50m MAS visible imagery shows a few isolated small clouds (<0.5km across) during the SW leg. The radiometric impact of these clouds in the HIRS/3 channel radiances is considered negligible. The clouds seen were off-nadir and will not affect the HIS measurements. For the NAST-I, co-location of the instrument footprint with the MAS imagery will allow the cloud contaminated spectra to be identified and removed.

The HIRS/3 channel 8 (11.11μm) IR window channel brightness temperatures for the July 11 mission are shown in figure 2. Unfortunately, the instrument entered into a calibration sequence during the overpass so only half of both the NE and SW ER-2 leg are covered by the HIRS/3 measurements. However, the brightness temperatures are very uniform in the region of interest, varying by only a few Kelvin over about 200km.

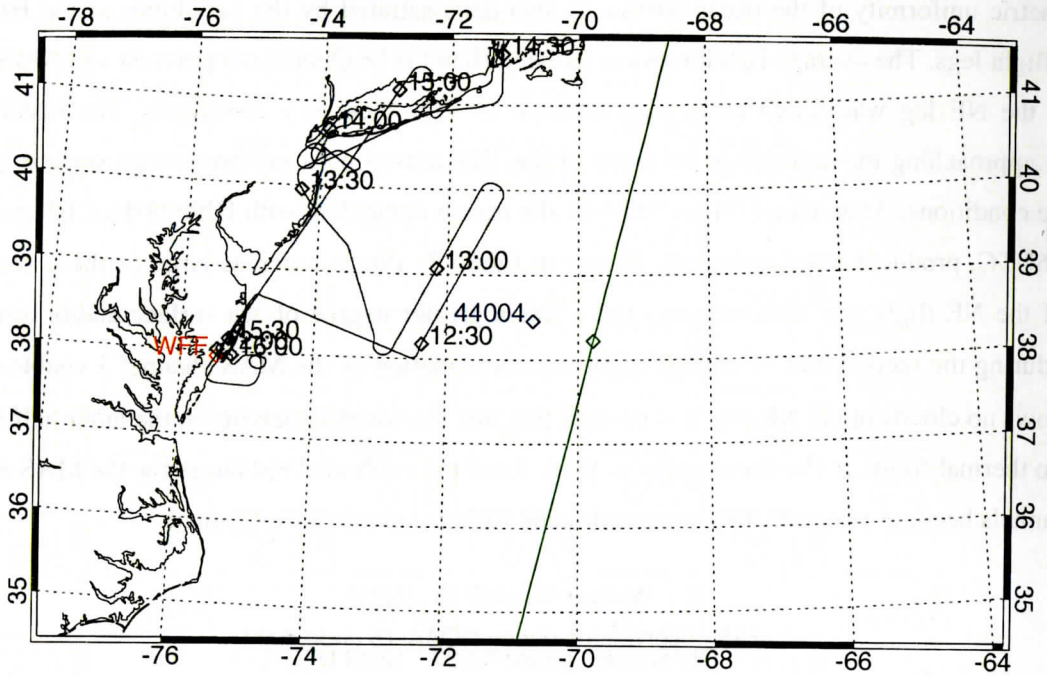

Figure 1. NOAA-15 nadir track and ER-2 flight track for July 11, 1998 mission. The mark in the nadir track is for 12:37:08UTC. The point labeled 44004 is the location of a NDBC buoy.

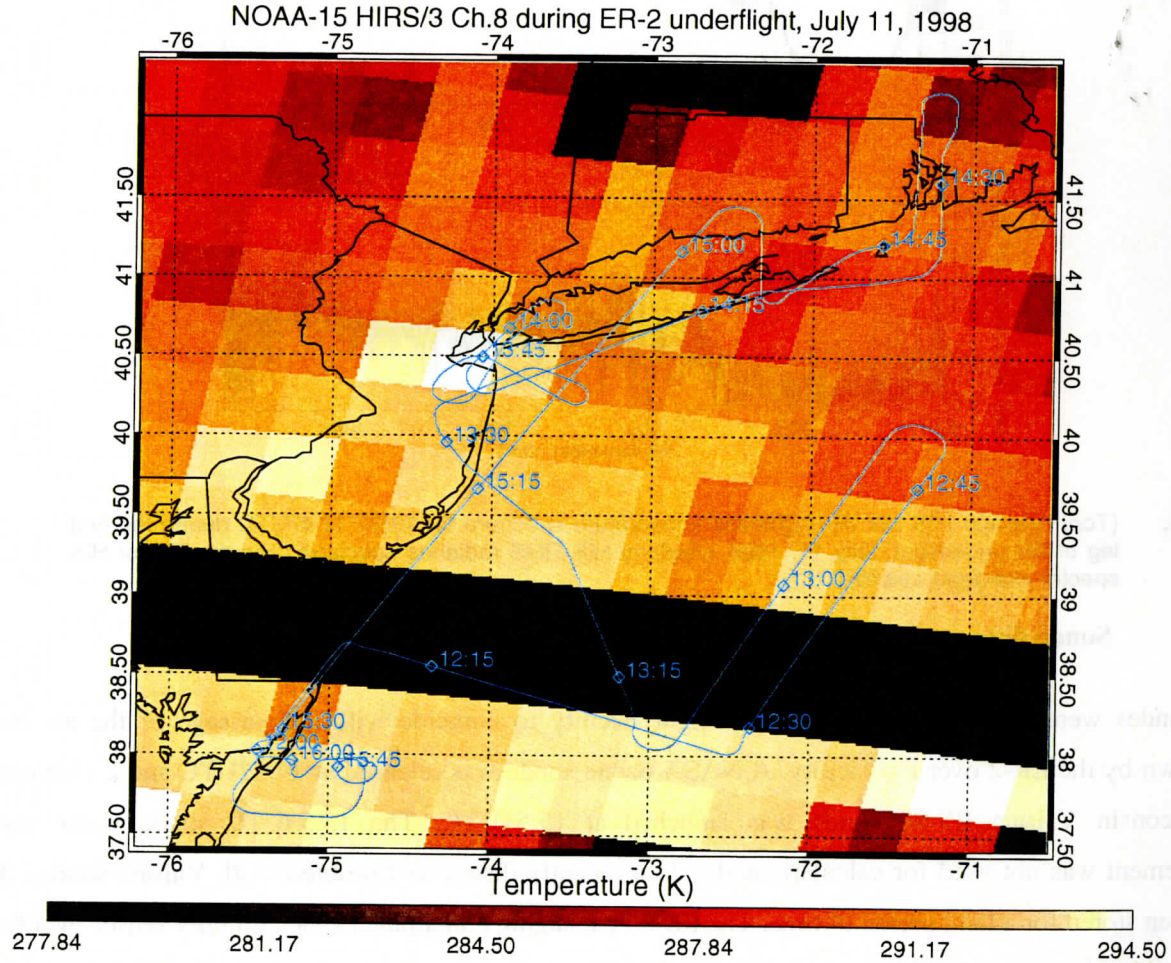

Figure 2. NOAA-15 HIRS/3 channel 8 image during ER-2 underflight. The aircraft and satellite were temporally co-located at 12:37UTC, the middle of the first leg.

The radiometric uniformity of the ocean surface is also demonstrated by the variability of the HIS spectra during the flight legs. The average HIS longwave IR band (band I) brightness temperature and RMS radiance spectra for the NE leg was found to be characteristic of very clear sky conditions. The RMS radiance variation is approaching the calibration accuracy of the HIS indicating a uniform ocean surface and stable atmospheric conditions. Averaging HIS spectra over the region coincident with HIRS/3 data, 62 spectra from 12:37-12:46UTC, produces RMS radiances, shown in figure 3, almost twice as large as those seen for the first half of the NE flight leg. This suggests there was a greater degree of sea surface and/or atmospheric variability during the second half of the NE flight leg. Examination of the MAS channel 3 visible (0.65μm) imagery shows no clouds in the NE leg. It is thought that this increased variability in the latter half of the NE leg is due to thermal fronts in the ocean surface. If so, when the calibrated radiances for the MAS shortwave thermal channels become available, this increased scene variance should be explained.

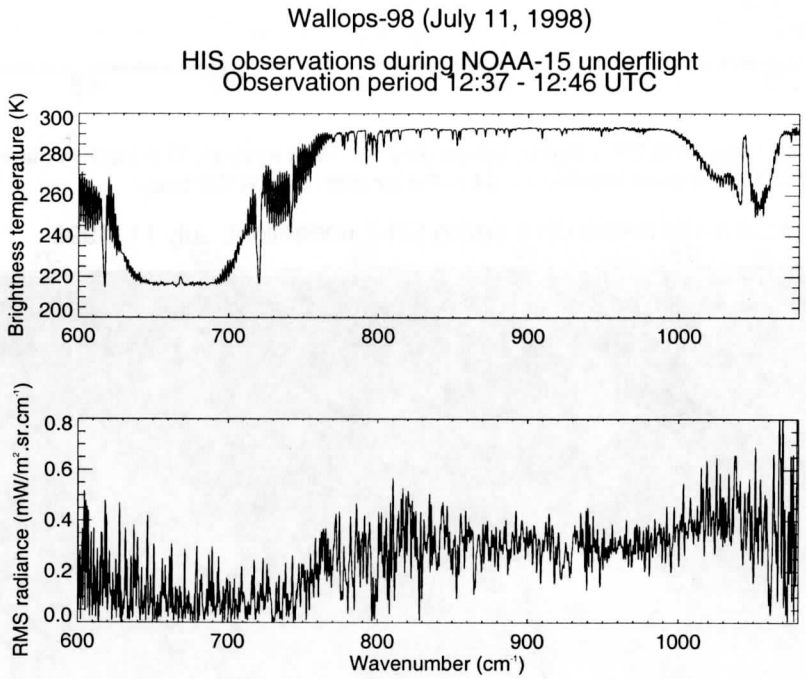

Figure 3. (*Top*) Average HIS LW IR brightness temperature spectrum for 12:37-12:47UTC during the first leg of the underflight, July 11, 1998. (*Bottom*) HIS RMS radiance spectrum. The number of HIS spectra averaged was 62.

3.2 Sonde data

Two sondes were released at the Wallops Flight Facility to coincide with the passage of the air mass overflown by the ER-2 over the facility. A NASA ozone sonde was released at 14:52UTC and a University of Wisconsin Vaisala RS-80 sonde was launched at 15:54UTC. The 15:54UTC sonde water vapor measurement was not used for calculations due to a recently discovered problem with Vaisala sondes that have been stored for a long period of time. The RS-80 packaging contaminates the humidity sensor over time and the older the sonde, the greater the contamination. This led to corrections of greater than 20% for the RS-80 relative humidity measurement. It was felt that a correction of this magnitude using an algorithm that has not been released to the scientific community invalidated the use of this sonde's data for the validation

exercise. The NASA ozone sonde was of a different type that did not suffer from the relative humidity contamination problem and thus was used in the forward model calculations.

4. CALCULATIONS

4.1 Sea surface emissivity

To model the satellite and aircraft measurements as accurately as possible, forward calculations were performed incorporating a computed sea surface emissivity in the radiative transfer using the algorithm described by *Wu and Smith* (1997). This algorithm is similar to that of *Masuda et al* (1988) except that it takes into account the reflected emission from the sea surface. Sea surface emissivities were calculated for view angles of 0.0, 11.22, and 13.25° and winds speeds of 1.0 and 2.0ms^{-1}. The non-zero angles represent the spread of view angles of the HIRS/3 over the ER-2 underflight area and the wind speeds were obtained from nearby (see figure 1) buoy measurements temporally collocated with the aircraft/satellite overpass. Figure 4 shows the calculated sea surface emissivity for a nadir view and 1.0ms^{-1} wind speed. The emissivity variation across the range of view angles and wind speeds was only 10^{-4}-10^{-5} in the HIS band I spectral region.

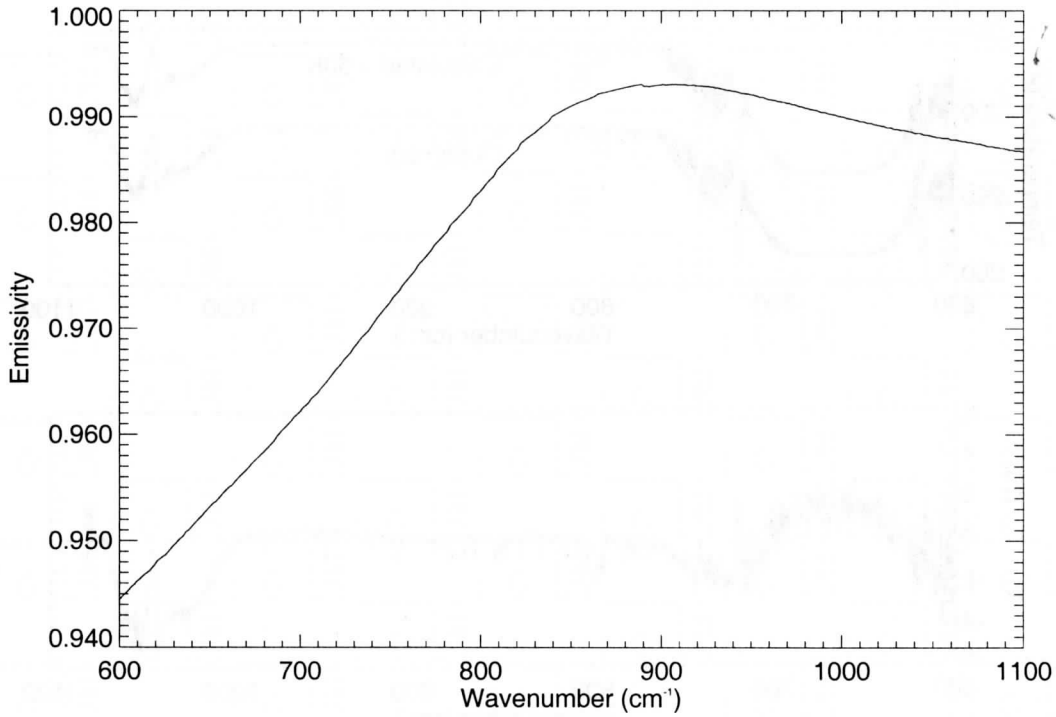

Figure 4. Calculated sea surface emissivity in the HIS band I spectral region for a view angle of 0.0° (nadir) and a wind speed of 1.0ms^{-1}.

4.2 HIS calculations

The HIS measurement was simulated by,

$$R_{HIS} = R_{atm}\downarrow \cdot\left(1-\varepsilon_{sfc}\right)\cdot\tau\left(p\rightarrow p_{ER-2}\right)+B\left(T_{sfc}\right)\cdot\varepsilon_{sfc}\cdot\tau\left(p\rightarrow p_{ER-2}\right)+R_{atm}\uparrow \qquad (3)$$

where $R_{atm}\downarrow$ = downwelling atmospheric radiance,

ε_{sfc} = calculated sea surface emissivity,

$\tau\left(p_{sfc} \rightarrow p_{ER-2}\right)$ = atmospheric transmittance from surface to ER-2 altitude,

$B\left(T_{sfc}\right)$ = Planck radiance for a given surface temperature, and

$R_{atm}\uparrow$ = upwelling atmospheric radiance.

All atmospheric transmittance calculations were performed using LBLRTM (*Clough and Iacono*, 1995) and the NASA sonde temperature, relative humidity, and ozone concentration profiles.

The buoy water temperature measurement for the overflight time was 294.05K however the best agreement between the average observed and calculated HIS spectra in the band I window region was for a surface temperature of 293.43K. The buoy measurement of water temperature is made one meter below sea level and, given that the temperature gradient in the first few millimeters of water can be large due to evaporative cooling (e.g. 0.2-0.6K, *Katsaros et al*, 1976), it was felt that adjustment of the surface skin temperature by 0.6K was reasonable. The HIS observed and calculated spectra and their difference are shown in figure 5.

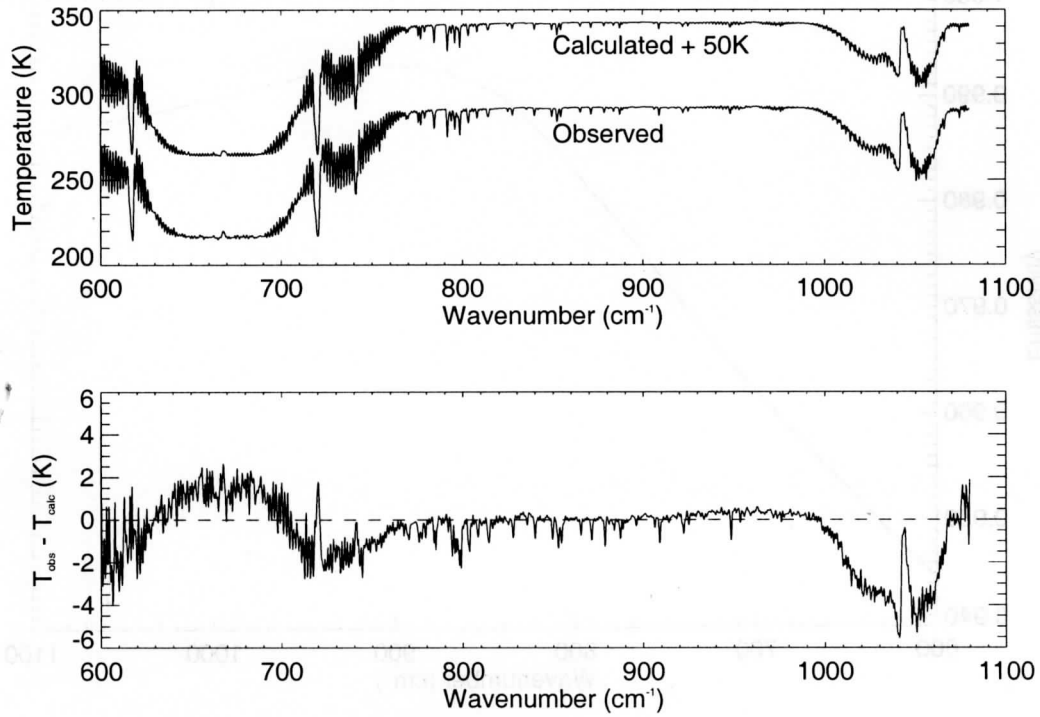

Figure 5. (*Top*) Comparison of HIS band I average observed (62 spectra, July 11 12:37-12:46UTC) and calculated +50K brightness temperature spectra and (*Bottom*) the observed minus calculated temperature residual spectrum.

The temperature residual spectrum in figure 5 suggests that,

- The water vapor profile used in the forward calculation may not be the best representation. In addition to the obvious on-line residuals for water vapor lines in the window region (e.g. at 800cm^{-1}), there is still a discernible slope in the brightness temperature difference from 800-1000cm^{-1} that is most likely due to the water vapor continuum contribution,

- The sonde mid-tropospheric temperature profile is too warm as shown by the –2K to –3K residuals from 600-610 and 710-760cm^{-1}, and
- The sonde upper-tropospheric temperature profile is too cold as shown by the +2K residuals in the 650-690cm^{-1} spectral region.

4.3 HIRS/3 calculations

The HIRS/3 simulations were performed in the same fashion as for the HIS (eqn. 3) except that the top pressure used in the forward calculation was decreased to 0.1mb. The sea surface temperature that provided the best result in the HIS longwave window was used and above the sonde profile mid-latitude summer climatology was used. Separate calculations were performed for each HIRS/3 FOV within the ER-2 underflight area; a 4×3 (across × along track) grid of HIRS/3 observations. Figure 6 shows the calculated and observed HIRS/3 channel 1-10 temperatures superimposed over the high resolution spectrum used to generate the calculated values and the observed minus calculated temperature residuals.

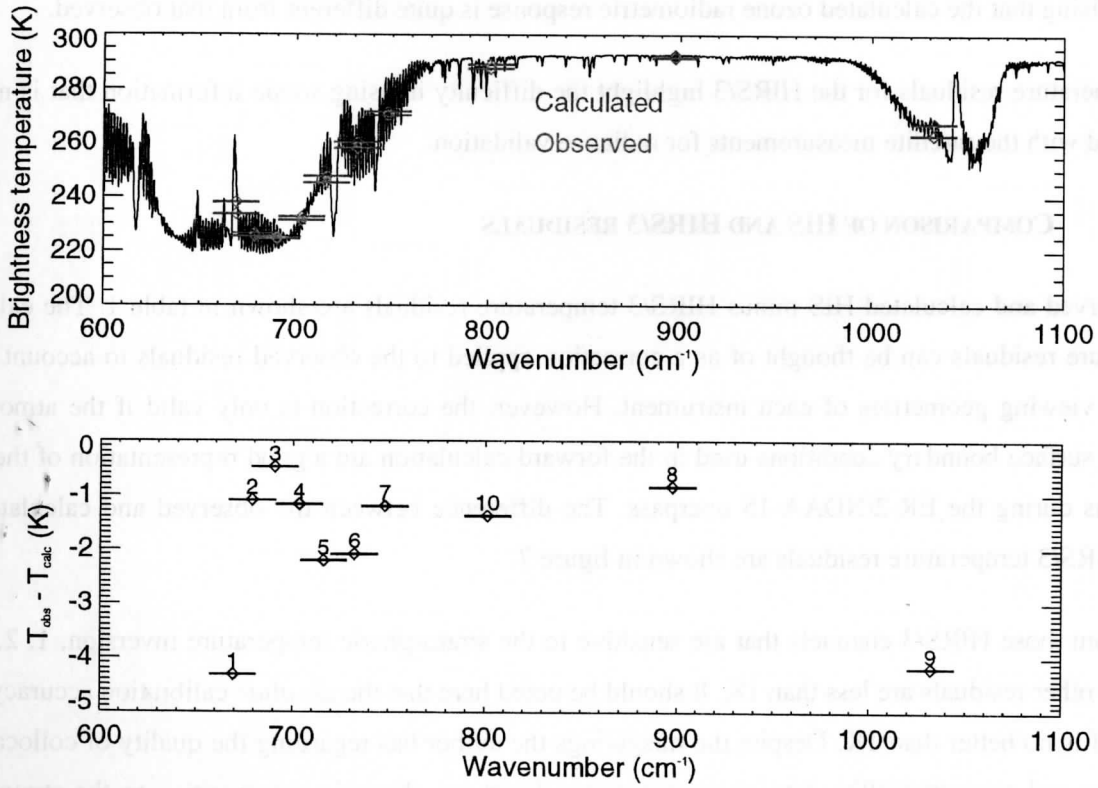

Figure 6. (*Top*) Comparison of HIRS/3 channel 1-10 average observed (12 FOVs) and calculated brightness temperatures overlaid on a high resolution calculation and (*Bottom*) the observed minus calculated temperature residuals. Note that the width of the channel symbols is *not* a true indication of the SRF fullwidth. The channel center frequency is indicated by the ◆ symbol. The corresponding channel numbers are shown in the bottom plot.

Keeping in mind the HIS residuals shown in figure 5, the HIRS/3 temperature residuals in figure 6 can be analysed by channel:

- *Channels 1, 2, and 3* - the large differences are due to a poor representation of the atmospheric state above the sonde top pressure (approximately 10mb). This is most evident for HIRS channel 1 effectively

invalidating the assumption that mid-latitude summer climatology was representative of the upper atmospheric state for this case. The expected, larger, negative channel 2 and 3 residuals are offset by the effect of the upper tropospheric temperature profile being too cold (which produced positive residuals for the HIS),

- *Channel 4* – this channel's response peaks in between the effect of the suspected too cold upper tropospheric and too warm mid-tropospheric temperature profile,
- *Channels 5, 6, and 7* – residuals of –2 to –1K are due to the effect of the too warm mid-tropospheric temperature profile producing similar values as seen for the HIS,
- *Channels 8 and 10* – the residuals of –1K suggest poor representation of the temperature profile near the sea surface. In addition, channel 10 is sensitive to lower level water vapor indicating a problem with the representativeness of the sonde water profile, and
- *Channel 9* – the large residual indicates the ozone concentration profile is not correct. Given the sonde/underflight collocation and the fact that that ozone can vary markedly over time and space it is not surprising that the calculated ozone radiometric response is quite different from that observed.

The temperature residuals for the HIRS/3 highlight the difficulty in using sonde information that is not well collocated with the satellite measurements for radiance validation.

5. COMPARISON OF HIS AND HIRS/3 RESIDUALS

The observed and calculated HIS minus HIRS/3 temperature residuals are shown in table 1. The calculated temperature residuals can be thought of as a correction applied to the observed residuals to account for the different viewing geometries of each instrument. However, the correction is only valid if the atmospheric state and surface boundary conditions used in the forward calculation are a good representation of the actual conditions during the ER-2/NOAA-15 overpass. The difference between the observed and calculated HIS minus HIRS/3 temperature residuals are shown in figure 7.

Apart from those HIRS/3 channels that are sensitive to the stratospheric temperature inversion, 1, 2, and 3, all of the other residuals are less than 1K. It should be noted here that the *absolute* calibration accuracy of the HIS itself is no better than 1K. Despite the misgivings the author has regarding the quality of collocation of the in situ and aircraft/satellite data, the comparisons for those channels not sensitive to the stratospheric temperature profile are quite favorable.

The relatively good agreement between the observed and calculated residuals shown in figure 7 notwithstanding, this plot on its own does not tell the complete story for channel 9 – the ozone channel. One cannot necessarily assume that a small residual *on its own* is evidence of good correspondence between the aircraft and satellite measurements. The <1K residual for channel 9 emphasises this fact. The poor agreement between the observations and calculations for both instruments (see figures 5 and 6) show that the ozone profile used in the forward calculation is not correct. However, the magnitudes of the errors are similar and

offset each other in figure 7. More work needs to be done to understand the sensitivity of the residual comparison for HIRS channel 9 to errors both in the total column ozone profile *and* the upper atmosphere temperature profile. Based on experience with ground-based interferometer ozone retrievals, it may be that the ozone and temperature profile errors offset each other in the satellite case leading to what appears to be a favorable comparison with the aircraft measurement. The other HIRS/3 longwave channels (1-8, 10) are either effectively transparent or are opaque to various degrees *due to one factor only* – in this case temperature. Thus it is not thought that the same ambiguity applies and the residuals shown in figure 7 for these channels are representative of the absolute calibration accuracy of the HIRS/3 – with the caveat of in situ data collocation, or lack thereof.

HIRS/3 channel	***HIRS/3 central wavenumber (cm^{-1})***	***Observed HIS – HIRS ΔT (K)***	***Calculated HIS – HIRS ΔT (K)***
1	669.180	-16.367	-21.893
2	678.812	-8.687	-11.320
3	690.479	-6.060	-7.627
4	703.196	-1.316	-2.329
5	715.982	0.527	-0.488
6	731.793	1.116	0.663
7	747.712	0.764	0.719
8	897.415	0.854	0.036
9	1032.188	5.920	5.024
10	801.155	0.949	0.203

Table 1. Temperature residuals between observed and calculated HIS, convolved with the HIRS/3 spectral response functions, and HIRS/3. The calculated temperature residuals can be thought of as a correction applied to the observed residuals to account for the different viewing geometries of each instrument.

6. CONCLUSIONS

The temperature residuals for the clear sky comparison of HIS and HIRS/3 longwave data shown in figure 7 do not represent an optimum scenario for vicarious calibration of the HIRS/3 using the HIS. The final residuals are relatively small for most channels, <1K, but given the uncertainties in the in situ data used in the forward calculations, a definitive statement as to the absolute calibration accuracy of the HIRS/3 cannot be made. Although an obvious point, this case study highlights the strict requirement that spatial and temporal collocation of the in situ data is a necessity for direct comparisons of satellite and aircraft radiance measurements to be made. However, as stated previously, apart from the stratospheric temperature channels – which still can be further corrected – the comparisons are thought to be indicative of truth and, with more rigorous attention to in situ data collection – e.g. sea surface temperature – would most likely improve. A preferred plan for vicarious calibration of satellite instruments with aircraft measurements would involve direct and indirect measurements of sea surface and atmospheric conditions at the target site (for example,

see *Smith et al*, 1996). In addition, a regular series of these types of measurements would provide a better picture of the quality of any one particular comparison and also an idea of the satellite sensor accuracy over its lifetime – one case study does not make a good statistical sample.

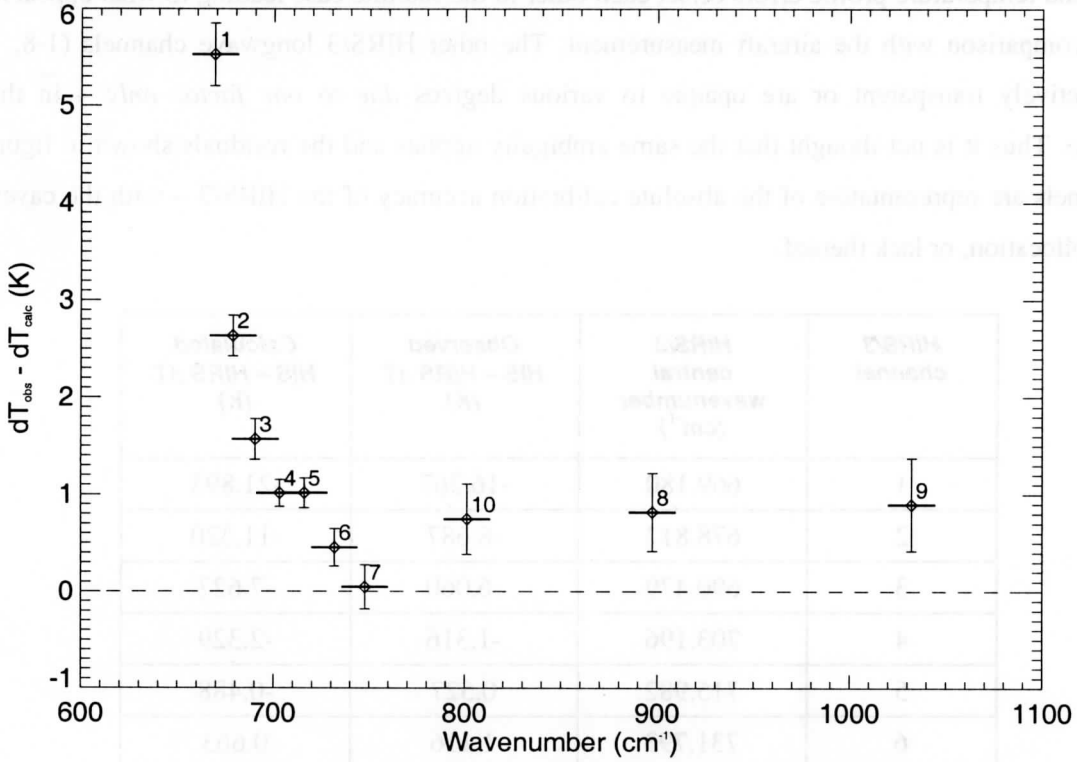

Figure 7. Observed minus calculated temperature residuals for HIS and HIRS/3. The dT in the ordinate axis label refers to the difference between the HIS and HIRS brightness temperatures, so $dT_{obs} - dT_{calc} = (T_{HIS} - T_{HIRS})_{obs} - (T_{HIS}-T_{HIRS})_{calc}$.

Further work to be carried out on the Wallops98 dataset involves the use of UARS HALOE data to supplement the upper atmospheric state profiles. Also, use of NCEP model output for the forward calculations should provide some information on how representative the sonde profile is of the atmosphere under observation. When NAST-I data becomes available, the analysis will be repeated but using the full spectral range of the NAST-I instrument. This will provide information on the mid- and shortwave channel HIRS/3 calibration.

In addition to the Wallops98 field experiment, clear sky over ocean measurements were taken with the Scanning-HIS and Millimeter Imaging Radiometer (MIR) during a field deployment in December, 1998. The Scanning-HIS data will allow a comparison, similar to that detailed here, to be made with the HIRS/3 and the MIR, with channel center frequencies identical to that of the AMSU-B, will allow characterisation of the AMSU-B instrument also. Also, during the WINTEX deployment in March 1999, the NAST-I, NAST-Microwave Temperature Sounder (MTS) and Scanning-HIS will be used to underfly NOAA-15 if the opportunity presents itself. The NAST-MTS has channels similar to some AMSU-A channels.

7. ACKNOWLEDGMENTS

This work was funded under NOAA Grant NA67EC0100.

8. REFERENCES

Clough, S.A. and M.J. Iacono, 1995. Line-by-line calculations of atmospheric fluxes and cooling rates. 2: Applications to carbon dioxide, ozone, methane, nitrous oxide and the halocarbons. *Journal of Geophysical Research*, **100**, pp16519-16535

Cousins. D. and W.L. Smith, 1997. National Polar-Orbiting Operational Environmental Satellite System (NPOESS) Aircraft Sounder Testbed – Interferometer (NAST-I). *SPIE*, **3127**, pp323-331.

Katsaros, K.B., W.T. Liu, J.A. Businger, and J.E. Tillman, 1976. Heat transport and thermal structure in the interfacial boundary layer measured in an open tank of water in turbulent free convection. *Journal of Fluid Mechanics*, **83** Part 2, pp311-335

Masuda, K., T. Takashima, and Y. Takayama, 1988. Emissivity of pure and sea waters for the model sea surface in the infrared window regions. *Remote Sensing Environment*, **24**, pp313-329

Revercomb, H.E., H. Buijs, H.B. Howell, D.D. LaPorte, W.L. Smith, and L.A. Sromovsky, 1988. Radiometric calibration of IR Fourier transform spectrometers: solution to a problem with the High-Resolution Interferometer Sounder. *Applied Optics*, **27**, pp3210-3218

Revercomb, H.E. V.P. Walden, D.C. Tobin, J. Anderson, F.A. Best, N.C. Ciganovich, R.G. Dedecker, T. Dirkx, S.C. Ellington, R.K. Garcia, R. Herbsleb, R.O. Knuteson, D.D. LaPorte, D. McRae, and M. Werner, 1998. Recent results from two new aircraft-based Fourier-transform interferometers: The Scanning High-resolution interferometer sounder and the NPOESS aircraft sounder testbed interferometer, 8th International Workshop on Atmospheric Science from Space using Fourier Transform Spectrometery (ASSFTS), Toulouse, France, 16-18 November 1998.

Smith, W.L. R.O. Knuteson, H.E. Revercomb, W. Feltz, H.B. Howell, W.P. Menzel, N. Nalli, O.B. Brown, J. Brown, P.J. Minnett, and W. McKeown, 1996. Observations of the infrared radiative properties of the ocean – implications for the measurement of sea surface temperature via satellite remote sensing, *Bulletin of the American Meteorological Society*, **77**, pp41-51.

Wu, X. and W.L. Smith, 1997. Emissivity of rough sea surface for 8-13μm: modeling and verification. *Applied Optics*, **36**, pp2609-2619

TECHNICAL PROCEEDINGS OF THE TENTH INTERNATIONAL ATOVS STUDY CONFERENCE

Boulder, Colorado

27 January - 2 February 1999

Edited by

J. Le Marshall and J.D. Jasper

Bureau of Meteorology Research Centre, Melbourne, Australia

Published by

Bureau of Meteorology Research Centre

PO Box 1289K, GPO Melbourne, Vic., 3001, Australia

December 1999